

Broadband spectroscopy of the eclipsing high mass X-ray binary 4U 1700-37 with Suzaku

Gaurava K. Jaisawal^{1*} and Sachindra Naik^{1†}

¹*Astronomy and Astrophysics Division, Physical Research Laboratory, Navrangpura, Ahmedabad - 380009, Gujarat, India*

ABSTRACT

We present the results obtained from broadband spectroscopy of the high mass X-ray binary 4U 1700-37 using data from a *Suzaku* observation in 2006 September 13-14 covering 0.29-0.72 orbital phase range. The light curves showed significant and rapid variation in source flux during entire observation. We did not find any signature of pulsations in the light curves. However, a quasi-periodic oscillation at ~ 20 mHz was detected in the power density spectrum of the source. The 1-70 keV spectrum was fitted with various continuum models. However, we found that the partially absorbed high energy cutoff power-law and Negative and Positive power-law with Exponential cutoff (NPEX) models described the source spectrum well. Iron emission lines at 6.4 keV and 7.1 keV were detected in the source spectrum. An absorption like feature at ~ 39 keV was detected in the residuals while fitting the data with NPEX model. Considering the feature as cyclotron absorption line, the surface magnetic field of the neutron star was estimated to be $\sim 3.4 \times 10^{12}$ Gauss. To understand the cause of rapid variation in the source flux, time-resolved spectroscopy was carried out by dividing the observation into 20 narrow segments. The results obtained from the time-resolved spectroscopy are interpreted as the accretion of inhomogeneously distributed matter in the stellar wind of the supergiant companion star as the cause of observed flux variation in 4U 1700-37. A sharp increase in column density after ~ 0.63 orbital phase indicates the presence of an accretion wake that blocks the continuum and produces the eclipse like low-flux segment.

Key words: X rays: stars: binaries: eclipsing – neutron – stars: individual – 4U 1700-37 – stars: individual – HD 153919

1 INTRODUCTION

4U 1700-37 was discovered by *Uhuru* satellite in December 1970 (Jones et al. 1973). Extensive follow-up observations with *Uhuru* revealed the system as an eclipsing binary with an orbital period of 3.412 days. One of the most luminous and hottest optical star among the known high mass X-ray binaries, a supergiant star (HD 153919) of O6.5 Iaf spectral type was identified as the optical companion (Hutchings et al. 1973). Using *BATSE* data, the orbital parameters of the binary system such as inclination $i=66^\circ$, eccentricity $e < 0.01$, $48 < a_x \sin i < 82$ lt-sec and semi eclipse angle $\theta_E=28^\circ.6$ were derived (Rubin et al. 1996). Using Monte Carlo simulation, the mass of compact object and mass and radius of the optical companion star were constrained at $M_x \sim 2.6 M_\odot$, $M_o \sim 30 M_\odot$ and $R_o \sim 18 R_\odot$, respectively (Rubin et al. 1996). Using ultraviolet and

optical spectroscopic observations, Clark et al. (2002) evaluated physical parameters of the optical companion and used in Monte Carlo simulation to estimate the mass of the X-ray source and optical companion to be $M_x \sim 2.44 \pm 0.27 M_\odot$ and $M_o \sim 58 \pm 11 M_\odot$. The distance of the binary system was estimated to be 1.9 kpc (Ankay et al. 2001).

A tentative detection of pulsation at ~ 67 s was reported from *Tenma* observations of 4U 1700-37 (Murakami et al. 1984). However, later observations did not confirm the detection of spin period in the source. Although detection of X-ray pulsations are not yet confirmed, the spectrum of 4U 1700-37 has been well described by the standard continuum models of the accretion powered X-ray pulsars. Broad-band X-ray spectrum of 4U 1700-37 obtained from various observatories such as *HEAO 1*, *EXOSAT*, *Ginga*, *BeppoSAX* had been described with a high energy cutoff power-law model (White et al. 1983; Haberl et al. 1989; Haberl & Day 1992; Reynolds et al. 1999). A soft excess component was also detected in the spectrum during the eclipse and eclipse ingress observations of 4U 1700-37 (Haberl et al. 1989; Haberl & Day

* gaurava@prl.res.in

† snaik@prl.res.in

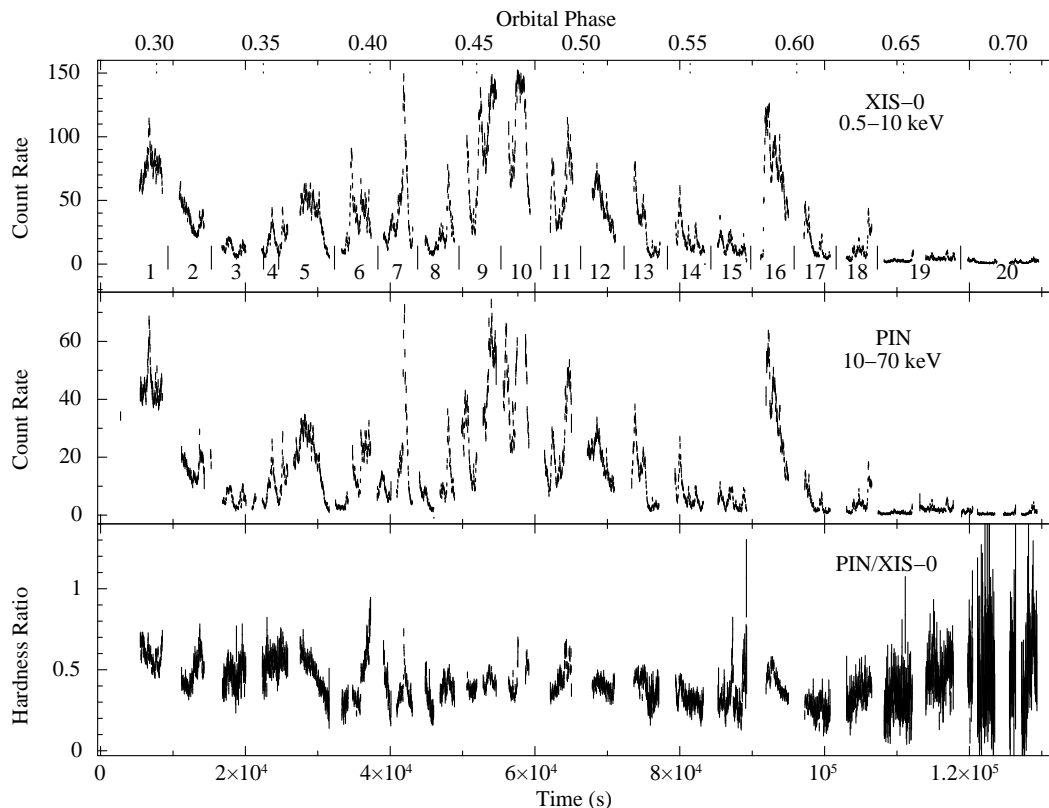


Figure 1. Light curves (top and middle panels) and hardness ratio (bottom panel) obtained from the *Suzaku* observation of the high-mass X-ray binary 4U 1700-37. Data from XIS-0 and HXD/PIN detectors are plotted here. Flux variability by an order of ~ 10 -15 can be seen in top and middle panels of the figure. The quoted numbers at the top panel show the duration of segments used for time-resolved spectroscopy. The orbital phases covered during the *Suzaku* observation are marked at the top of the figure.

1992). 1991 April *Ginga* observation of the source showed a clear difference in the temperature corresponding to the soft excess component before and after the eclipse (0.47 keV and 0.74 keV). The rise in soft excess temperature after the eclipse was explained on the basis of the bow shock formation in front of compact object (Haberl et al. 1994).

The nature of the compact object in 4U 1700-37 binary system is quite unclear. Due to observed hard X-ray spectrum and non-detection of pulsation, Brown et al. (1996) suggested the X-ray source as a low mass black hole candidate. However, the 2-200 keV *BeppoSAX* spectrum of 4U 1700-37 was found to be well fitted with a high energy cutoff power-law model representing the classical spectrum of an accretion powered X-ray pulsars (Reynolds et al. 1999). Apart from this, Reynolds et al. (1999) also reported the possible presence of cyclotron absorption feature at ~ 37 keV in *BeppoSAX* spectrum. These results discarded the possibility of a black hole as a compact object in the 4U 1700-37 binary system. High resolution spectra from *Chandra* and *XMM-Newton* observatories were described by using two component absorption model as used in 1991 April *Ginga* observation (Boroson et al. 2003; van der Meer et al. 2005). The recombination lines from H and He like species and fluorescence emission lines from neutral atoms were seen in the *Chandra* observations during intermittent flare state of 4U 1700-37. The strength of the lines were found to be varying over the observation. The detection of triplet structure in Si and Mg indicated the disequilibrium of the photo-ionized

plasma (Boroson et al. 2003). Many recombination lines as well as fluorescence emission lines were also detected in the spectrum of *XMM-Newton* observation of 4U 1700-37 during eclipse, eclipse egress and low flux segments of the binary (van der Meer et al. 2005). Presence of recombination lines from H and He atoms in eclipse phase suggested an extended ionization region around the source. As in the case of accretion powered X-ray pulsars, several mHz QPOs were also detected in the power density spectra of 4U 1700-37, obtained from the *Chandra* observation (Boroson et al. 2003).

4U 1700-37 was observed by *Suzaku* in 2006 September during out of eclipse phase of the binary. We report the time-averaged and time-resolved broadband spectroscopy of 4U 1700-37 to understand the nature of the continuum emission and its orbital dependency, flaring activities, emission lines and cyclotron features in the spectrum.

2 OBSERVATION AND ANALYSIS

Suzaku is the fifth Japanese X-ray satellite which was launched in 2005 July by Japan Aerospace Exploration Agency (Mitsuda et al. 2007). It covers a broad energy range (from 0.2 keV to 600 keV) in the X-ray band with the help of two sets of detectors, X-ray Imaging Spectrometers (XIS; Koyama et al. 2007) and Hard X-ray Detectors (HXD; Takahashi et al. 2007). XISs are imaging CCD cameras that work

in 0.2-12 keV range. Three CCD cameras (XIS-0, XIS-2 and XIS-3) are front-illuminated whereas the other one (XIS-1) is back-illuminated. The effective areas of front-illuminated and back-illuminated XISs are 340 cm² and 390 cm² at 1.5 keV, respectively. Field of view of XIS is 18' × 18' in full window mode. HXD is a non-imaging detector consisting of two instruments such as silicon PIN diodes (HXD/PIN) and GSO crystal scintillators (HXD/GSO) working in 10-70 keV and 40-600 keV ranges, respectively. Effective area of the HXD/PIN is 145 cm² at 15 keV whereas for GSO, it is 315 cm² at 100 keV. Field of view of HXD/PIN is 34' × 34' and is similar for HXD/GSO up to 100 keV.

4U 1700-37 was observed with *Suzaku* in 2006 September 13-14. The observation was carried out during out of eclipse phase of the binary covering 0.29-0.72 orbital phase range (considering mid-eclipse time as phase zero; Rubin et al. 1996). The observation was performed in “XIS nominal” position with an effective exposure of ~81.5 ks and ~82.1 ks for XIS and HXD, respectively. XIS detectors were operated in the “burst” clock mode with “1/4 window” option providing 1 s time resolution during the observation. We used publicly available data (version 2.0.6.13) of the *Suzaku* observation in the present work. HEASoft software package (version 6.12) and calibration database (CALDB) released on 2012 February 10 (for XIS) and 2011 September 13 (for HXD) were used for the data analysis.

Unfiltered event files were processed by using ‘aepipeline’ package of FTOOLS along with standard screening criteria to create cleaned XIS and PIN event files. These reprocessed clean event files were used in further analysis. “XSELECT” package of FTOOLS was used to extract light curves and spectra from the reprocessed XIS and HXD/PIN event data. Barycentric correction was applied on the reprocessed clean event files by using the task ‘aebarycen’. Attitude correction was applied to the reprocessed XIS event data files by using S-lang script *aeattcor.sl*¹. The reprocessed XIS event data were checked for the possible presence of photon pile-up. Photon pile-up in XIS event data was estimated by using S-lang script *pile_estimate.sl*² and found to be 10%, 11%, 11% and 11% at the center of the image obtained from XIS-0, XIS-1, XIS-2 and XIS-3 event data, respectively. An annulus region with inner and outer radii of 30" and 180" from the source position was selected to reduce the photon pile-up to ≤4%. Source light curves and spectra were extracted from the reprocessed XIS event data by selecting above annulus region around the central source. Background light curves and spectra were accumulated by selecting circular regions away from the source. The response and effective area files for all the XIS detectors were generated by using the task ‘xisrmfgen’ and ‘xissimarfgen’ of FTOOLS. Source light curve and spectra were created from reprocessed HXD/PIN event file by using “XS-ELECT”. However, the HXD/PIN background light curves and spectrum were accumulated in a similar manner from ‘tuned’ non X-ray background (NXB³) event file. A correction for cosmic X-ray background (CXB⁴) was incorporated

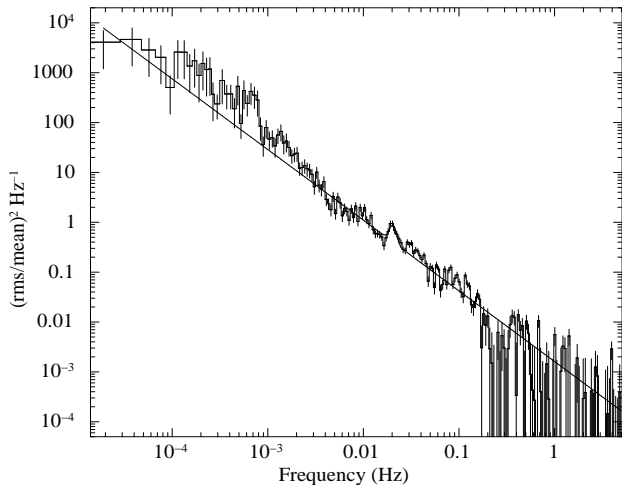


Figure 2. Power density spectrum (PDS) of 4U 1700-37 obtained from HXD/PIN light curve in 10-70 keV energy range. Absence of pulsations in the range of 10⁻⁵ Hz to 2 Hz range can be seen in the figure. A QPO at ~20 mHz is detected in the PDS of the X-ray source. The solid line in the figure represents the fitted model comprising of a power-law continuum and a Gaussian function at the QPO frequency.

in the PIN spectra as suggested by the instrument team. Epoch 2 response file (20080129) for HXD/PIN was used in the spectral analysis. Data from all four XISs (XIS-0, XIS-1, XIS-2 and XIS-3) and HXD/PIN were used in the present study.

3 RESULTS

Source and background light curves in soft (XIS - 1 s time resolution) and hard X-ray (HXD/PIN - 0.1 s time resolution) energy ranges were extracted as described above. Background subtracted light curves in 0.5-10 keV and 10-70 keV ranges are shown in top and middle panels of Figure 1. From the figure, significant and rapid flux variability by a factor of ~10-15 can be seen in soft and hard X-ray bands. The presence of flaring episodes along with stable low flux segments can also be clearly seen in XIS and PIN light curves. Hardness ratio (ratio between the light curves obtained from HXD/PIN and XIS-0 event data) plot (bottom panel of Figure 1) was generated to check the spectral state of the source during the flaring episodes as well as low flux segments in the light curve. However, apart from marginal hardening during the extended low flux segment towards the end of the observation, any significant change in the value of hardness ratio (spectral state) was absent.

To investigate the presence of any periodicity (pulsation) in the X-ray source, power density spectrum (PDS) was generated by using HXD/PIN light curve with 0.1 s time resolution and shown in Figure 2. Absence of any clear and sharp peaks in the PDS in 0.5 s to 10⁵ s range suggested the non-detection of pulsation in above time range. To confirm the non-detection of pulsation, we generated pulse profiles by assuming 50 s (corresponding to ~20 mHz peak in the PDS) and earlier reported 67 s (from *Tenma* observation) as the spin period of the source. We defined pulse fraction as the ratio between the difference in the maximum and mini-

¹ <http://space.mit.edu/ASC/software/suzaku/aeattcor.sl>

² http://space.mit.edu/ASC/software/suzaku/pile_estimate.sl

³ <http://heasarc.nasa.gov/docs/suzaku/analysis/pinbgd.html>

⁴ http://heasarc.nasa.gov/docs/suzaku/analysis/pin_cxb.html

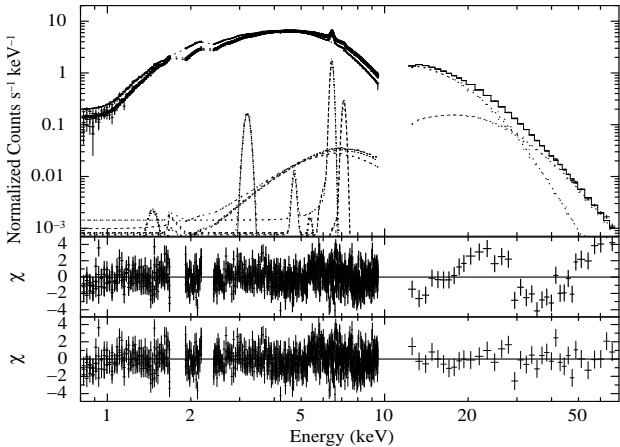


Figure 3. Energy spectrum of 4U 1700-37 obtained with the XISs and PIN detectors of the *Suzaku* observation, along with the best-fit model comprising a partial covering NPEX continuum model, three Gaussian functions for emission lines and a cyclotron absorption component. The middle and bottom panels show the contributions of the residuals to χ^2 for each energy bin for the partial covering NPEX continuum model without and with cyclotron component in the model, respectively.

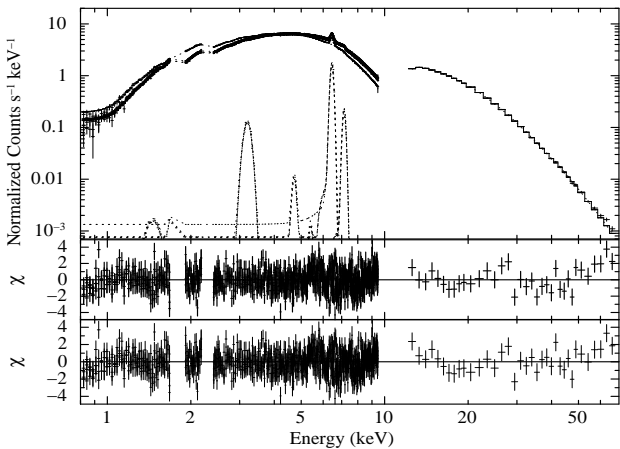


Figure 4. Energy spectrum of 4U 1700-37 obtained with the XISs and PIN detectors of the *Suzaku* observation, along with the best-fit model comprising a partial covering high energy cutoff power-law continuum model, three Gaussian functions for emission lines and a cyclotron absorption component. The middle and bottom panels show the contributions of the residuals to χ^2 for each energy bin for the partial covering power law continuum model without and with cyclotron component in the model, respectively.

imum intensities to the sum of the maximum and minimum intensities in the pulse profile. We estimated pulse-fraction from each of the pulse profiles obtained by assuming 50 s and 67 s as spin period of the source and found to be $\sim 1\%$. The negligible values of pulse fraction indicate the non-detection of X-ray pulsation in the source. On the other hand, the observed weak and broad feature at ~ 20 mHz confirmed the detection of a quasi-periodic oscillation (QPO) in the X-ray source. The significance of QPO feature was determined by fitting the PDS with a power-law continuum along with a Gaussian function at QPO frequency and found that the detection was more than 3σ level.

For spectral analysis, the source and background spectra, response matrices and effective area files for all instruments were generated by following the procedures described in previous section. After appropriate background subtraction, spectra from all the detectors were fitted simultaneously in 0.8-70 keV energy range using XSPEC v12.7 package. Due to the presence of known Si and Au edge feature in XIS spectra, data in 1.7-1.9 keV and 2.2-2.4 keV energy ranges were ignored in the spectral fitting. The XIS spectra were binned by a factor of 6 from 0.8 to 10 keV whereas the PIN spectrum was binned by a factor of 2 up to 25 keV, a factor of 4 from 25 keV to 50 keV and a factor of 6 from 50 to 70 keV. All the spectral parameters were tied together during the fitting except the relative normalization of detectors which were kept free. Standard continuum models for X-ray pulsars like high energy cutoff power-law (White, Swank & Holt 1983), Fermi Dirac cutoff power-law (FD-CUT; Tanaka 1986), NewHcut (a third order polynomial function with continuous derivatives; Burderi et al. 2000), cutoff power-law, NPEX (Makishima et al. 1999), Thermal Comptonization model (CompTT; Titarchuk 1994) were applied in the spectral fitting. However, the high energy cutoff power-law, NewHcut and NPEX model with partial covering component described the source spectrum well.

Addition of partial covering component to all three continuum models improved the spectral fitting yielding the reduced χ^2 values from >4 to <2 . In this model component, there are two different absorption components. One component (equivalent hydrogen column density along the source direction) absorbs the entire spectrum, whereas the other component (inhomogeneously distributed matter close to the X-ray source) absorbs the source spectrum partially. This model has been used to describe spectra of other HMXBs (Jaisawal et al. 2013; Pradhan et al. 2014) and Be/X-ray binary pulsars which show the presence of several absorption dips at various pulse phases during Type I outbursts (Naik et al. 2011; Paul & Naik 2011; Maitra et al. 2012; Naik et al. 2013 and references therein). Apart from these spectral components in the continuum models, the iron fluorescence lines at 6.42 keV (Fe K_α) and 7.1 keV (Fe K_β) were detected in the spectrum of 4U 1700-37. An emission line like feature at 3.19 keV was seen in the spectral residue of all three continuum models. Addition of a Gaussian component at ~ 3.19 keV to above three continuum models improved the spectral fitting further. The line at ~ 3.19 keV was identified as the fluorescence emission from S XV as seen in EXO 2030+375 (Naik et al. 2013) or Ar K_β .

In contrast to earlier findings, the thermal component (soft X-ray excess) was not seen in the spectrum during the *Suzaku* observation of 4U 1700-37. *XMM-Newton* observations of the source, however, showed the presence of soft X-ray excess over the continuum model in 0.22-0.31, 0.72-0.79 and 0.07-0.17 orbital phase ranges. Apart from the eclipse phase when two soft X-ray excess components were detected, the source showed a single and weak soft X-ray excess during other orbital phases (van der Meer et al. 2005). Though the source was observed with *XMM-Newton* at four epochs, only one observation (in 0.48-0.59 phase range) overlaps partly with the binary orbital phase covered during *Suzaku* observation. The non-detection of soft X-ray excess during *Suzaku* observation of the source, therefore, can be explained as due to the relatively low sensitivity of *Suzaku* instruments com-

Table 1. Best-fit parameters obtained from the spectral fitting of *Suzaku* observation of 4U 1700-37 with 90% errors. Model-1 : Partial covering NPEX model with Gaussian components, Model-2 : Partial covering NPEX model with Gaussian components and cyclotron absorption line, Model-3 : Partial covering high energy cutoff power-law model with Gaussian components, Model-4 : Partial covering high energy cutoff power-law model with Gaussian components and cyclotron absorption line, Model-5 : Partial covering NewHcut model with Gaussian components and Model-6 : Partial covering NewHcut model with Gaussian components and cyclotron line.

Parameter	Model-1	Model-2	Model-3	Value	Model-4	Model-5	Model-6
N_{H1}^a	1.9±0.1	2.0±0.1	2.2±0.3		2.2±0.1	2.2±0.1	2.2±0.1
N_{H2}^b	4.1±0.1	4.5±0.2	4.9±0.1		4.9±0.1	4.5±0.1	4.8±0.2
Cov. Fraction	0.6±0.1	0.6±0.1	0.7±0.1		0.7±0.1	0.7±0.1	0.7±0.1
Photon index	0.2±0.1	0.3±0.1	1.0±0.1		1.0±0.1	0.9±0.1	0.9±0.1
E_{cut} (keV)	7.5±0.1	8.8±1.5	7.1±0.1		7.1±0.1	7.0±0.2	7.0±0.2
E_{fold} (keV)	–	–	19.1±0.1		19.7±0.4	18.6±0.4	19.0±0.5
Fe K_α line							
Line energy (keV)	6.46±0.01	6.46±0.01	6.46±0.01		6.46±0.01	6.46±0.01	6.46±0.01
Eq. width (eV)	81±2	82±3	75±2		75±2	77±2	77±2
Fe K_β line							
Line energy (keV)	7.13±0.01	7.13±0.01	7.15±0.01		7.15±0.01	7.14±0.01	7.14±0.01
Eq. width (eV)	21±2	22±2	14±1		14±1	20±2	20±2
Cyclotron line							
Line energy (keV)	–	38.9±3.2	–		38.9*	–	38.9*
Width (keV)	–	19.3 ^{+6.1} _{-4.3}	–		9.8 ^{+8.1} _{-5.1}	–	7.3 ^{+8.3} _{-5.5}
Depth	–	0.4±0.1	–		0.1±0.1	–	0.1±0.1
Flux ^c (1-10 keV)	2.1±0.1	2.1±0.1	2.1±0.1		2.1±0.1	2.1±0.1	2.1±0.1
Flux ^c (10-70 keV)	5.6±0.3	5.7±0.7	5.6±0.2		5.6±0.1	5.6±0.2	5.6±0.2
Norm. Const. ^d	1/1/1.04/0.98/1.02	– – – –	1/1/1.04/0.98/1.02		– – – –	1/1/1.04/0.98/1.01	– – – –
χ^2 (dofs)	1551 (888)	1363 (885)	1389 (888)		1375 (886)	1349 (887)	1343 (885)

^a : Equivalent hydrogen column density in the source direction (in 10^{22} atoms cm^{-2} units),

^b : Additional hydrogen column density (10^{22} atoms cm^{-2} units),

^c : in 10^{-9} ergs cm^{-2} s^{-1} unit.

^d : Quoted relative normalization constants are for XIS-0, XIS-1, XIS-2, XIS-3 and PIN, respectively. The values remain same while adding CRSF with the respective continuum models (Model-1, Model-3 and Model-5).

* : The values were fixed at the value obtained from spectral fitting with Model-2.

pared to that of *XMM-Newton* to detect the weak soft component in the spectrum.

Apart from the soft X-ray excess, earlier reported absorption like feature at ~ 37 keV in the source spectrum (Reynolds et al. 1999) was also marginally seen in the spectral residuals of all three continuum models in the present work. However, the absorption feature was clearly detected when the source spectrum was fitted with partial covering NPEX continuum model. Addition of cyclotron absorption component to the partial covering NPEX continuum model improved the spectral fitting yielding better value of reduced χ^2 which was decreased from 1.75 to 1.54. Energy and width of the cyclotron absorption feature were found to be ~ 39 keV and ~ 19 keV, respectively. The cyclotron absorption component was added to the partial covering high energy cutoff power-law and NewHcut models yielding almost identical results. The parameters obtained from the spectral fitting of *Suzaku* observation of 4U 1700-37 are given in Table 1. The values of relative instrument normalizations of four XISs and HXD/PIN are also given in the table and found to be comparable to that obtained during the detector calibrations. The energy spectra of the source are shown in Figures 3 and 4 along with the best-fit models of partial covering NPEX model and partial covering high energy cutoff power-law model, respectively. The middle and bottom panels in each figure show the residuals to the best-fit models with

out and with the addition of cyclotron absorption line in the continuum model, respectively.

To check the statistical significance of the absorption feature, F-test routine of *IDL*, *mpftest*⁵, was applied on the χ^2 . As in case of 4U 1909+07 (Jaisawal et al. 2013), probability of chance improvement (PCI) was evaluated by considering the χ^2 without and with the cyclotron absorption component in continuum models (Press et al. 2007). The estimated PCI was found to be 3%, 46% and 49% after adding the cyclotron component in the partial covering NPEX model, the partial covering high energy cutoff power-law model and the partial covering NewHcut model, respectively. At such high PCI values (46% and 49%), the detection of cyclotron absorption feature is statistically insignificant in spectral fitting with partial covering high energy cutoff power-law and partial covering NewHcut models. Though the PCI value for partial covering NPEX model (3%) suggest the detection of cyclotron absorption feature in the source, the broad width of the feature (~ 19 keV) makes the detection tentative. Considering the different values of PCI obtained for different models, the use of F-test in checking the statistical significance of the presence of cyclotron absorption component in the spectrum of 4U 1700-37 (present case) may not be reliable enough. Observations with high

⁵ <http://www.physics.wisc.edu/~craigm/idl/down/mpftest.pro>

sensitive hard X-ray detectors for long exposures can confirm the presence/absence of cyclotron resonance scattering feature in 4U 1700-37.

3.1 Time-resolved spectroscopy

During the *Suzaku* observation of 4U 1700-37, observed source flux was found to be highly variable at different time scales. Several flare like episodes lasting for ~ 10 ks and low flux segments were seen in soft and hard X-ray light curves (Figure 1). To probe the changes in spectral parameters during these flaring episodes and low flux segments at such short intervals, we divided the entire observation into 20 segments as marked in the top panel of Figure 1. As mentioned earlier, source spectra for these 20 segments were extracted from all four XISs and PIN detectors. For time-resolved spectroscopy, we used same background spectra and response matrices for corresponding detectors that were used for time-averaged spectroscopy. As all three models used in time-averaged spectroscopy well fitted the source spectrum, we choose one of the model e.g. the high energy cutoff power-law model to fit the time-resolved spectra. Iron K_α and K_β lines were detected in each of the 20 time-resolved spectra. The best-fit spectral parameters (with 90% errors) obtained from the simultaneous spectral fitting of each of the segments are plotted in Figure 5 along with XIS-0 and PIN light curves in left and right top panels, respectively.

The equivalent hydrogen column density N_H was found to be high ($7 \times 10^{22} \text{ cm}^{-2}$) in the beginning of observation. However, the values of N_H gradually decreased to a low value beyond which again showed gradual increase during the observation. The systematic and smooth variation of N_H irrespective of source intensity during the *Suzaku* observation suggested the orbital dependence of the matter distribution in 4U 1700-37. This can be confirmed with further long observations of the source with upcoming observatories such as ASTROSAT. A sharp increase in the value of N_H ($13 \times 10^{22} \text{ cm}^{-2}$) was observed during the extended low flux segment towards the end of the observation (after ~ 0.63 orbital phase). The power-law photon index was found to be variable e.g. higher during the low flux segments compared to the flaring episodes.

Flux of Iron K_α and K_β emission lines were found to vary with the source flux whereas the corresponding equivalent widths showed the opposite trend. Source flux as well as the flux of iron emission lines were found to be low during the extended low flux segment at the end of the observation. The variation in the iron line parameters (flux and equivalent width) with the absorbed source flux in 8-70 keV are plotted in Figure 6. Though the flux of both the emission lines increased along with the source flux, flux of K_α line was found to increase faster compared to that of the K_β line. However, the equivalent width of both the lines showed no systematic variation with the source flux though the values were higher at low flux level. Dependence of emission line flux and equivalent width with the source flux indicates the fluorescence origin of the lines from the matter near by the neutron star. Variation of iron emission line flux and equivalent width with hard X-ray continuum flux (8-70 keV) in 4U 1700-37 are found to be similar to that found in LMX X-4 and Her X-1 (Naik & Paul 2003). In case of LMC X-4 and Her X-1, the change in iron line parameters

with continuum flux was interpreted as due to the presence of precessing tilted accretion disk causing modification in the geometry and visibility of iron line emitting region in the binary systems. To investigate the geometry in 4U 1700-37 binary system, we plotted the equivalent widths of 6.4 keV and 7.1 keV iron lines with the observed column density in Figure 7. The equivalent widths of both the lines are found to be marginally variable with the column density. Similar kind of variation of equivalent width (below of 200 eV) with absorption column density (order of 10^{22} cm^{-2}) was seen in Her X-1 and Vela X-1 (Figure 8 of Makishima et al. 1986). In such configuration, the X-ray source is expected to be surrounded by inhomogeneously distributed absorbing material that covers a fraction of radiation along the line of sight.

4 DISCUSSION

The continuum X-ray emission in the neutron star X-ray binaries is understood to be emitted through the inverse Comptonization of the photons originated from the magnetic poles as well as within the accretion column of the neutron star (Becker & Wolff 2007). The emitted photons interact with the materials present in the surroundings of the neutron star. The effect of interactions can be seen in the observed spectrum in the form of photo-electric absorption, soft excess emission, line emissions and cyclotron absorption features. Detection of soft excess and line emissions can reflect the reprocessing of hard X-ray photons with matter (neutral or ionized plasma) in accretion disk, accretion column etc. The effect of the neutron star magnetic field can be seen in the X-ray spectrum through the interaction of quantized electrons with the source photons. Depending on the strength of the neutron star magnetic field, the electrons are quantized in to Landau levels through the relation $E_a = 11.6 B_{12} (1 + z_g)^{-1}$ (keV), where z_g is gravitational red-shift and B_{12} is magnetic field strength in units of 10^{12} Gauss. The absorption like feature, cyclotron resonance scattering feature (CRSF), is detected generally in 10-100 keV spectrum. In the present case of high mass X-ray binary 4U 1700-37, we detected an absorption like feature at ~ 39 keV, as was earlier reported in *BeppoSAX* spectrum of the source (Reynolds et al. 1999). During the *BeppoSAX* observation, the cyclotron absorption feature was detected when the source spectrum was fitted with a high energy cutoff power-law model. However, in the present study, the cyclotron absorption feature was detected when the spectrum was fitted with a NPEX model. Though the detections of CRSF during *BeppoSAX* observation as well as *Suzaku* observation did not provide any concluding results, the presence of weak absorption-like feature at ~ 39 keV in both the cases can not be entirely ruled out. Assuming the detected feature as CRSF in 4U 1700-37, the magnetic field of the X-ray source (neutron star) in the binary system was estimated to be $\sim 3.4 \times 10^{12}$ Gauss. The presence of the cyclotron feature can be confirmed by using data from future observations with long exposure and good hard X-ray spectroscopic instruments such as *NuSTAR*, *ASTROSAT* & *Astro* – *H* missions.

4U 1700-37 was found to be significantly variable during the *Suzaku* observation. Such kind of flux variability are seen in other wind-accreting high mass X-ray binaries such

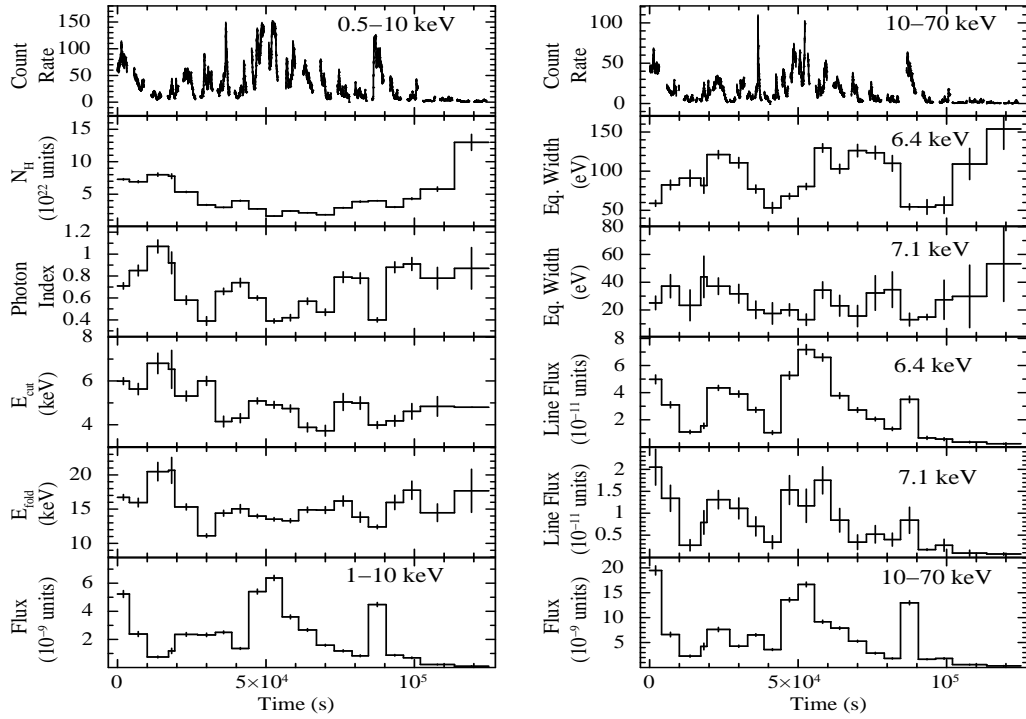


Figure 5. Spectral parameters obtained from the time-resolved spectroscopy for *Suzaku* observation of 4U 1700-37. The top panels in both the sides show light curves of 4U 1700-37 in 0.5-10 keV (XIS-0) and 10-70 keV (HXD/PIN) energy ranges. The values of N_H , power-law photon index, cutoff (E_{cut}) and folding energy (E_{fold}) are shown in second, third, fourth and fifth panels in left side, respectively. The iron emission line parameters such as the equivalent widths and flux in for 6.4 keV and 7.1 keV iron emission lines are shown in second, third, fourth and fifth panels in right side, respectively. The source flux in 1-10 keV (left side) and 10-70 keV (right side) are shown in bottom panels. The errors shown in the figure are estimated for 90% confidence level.

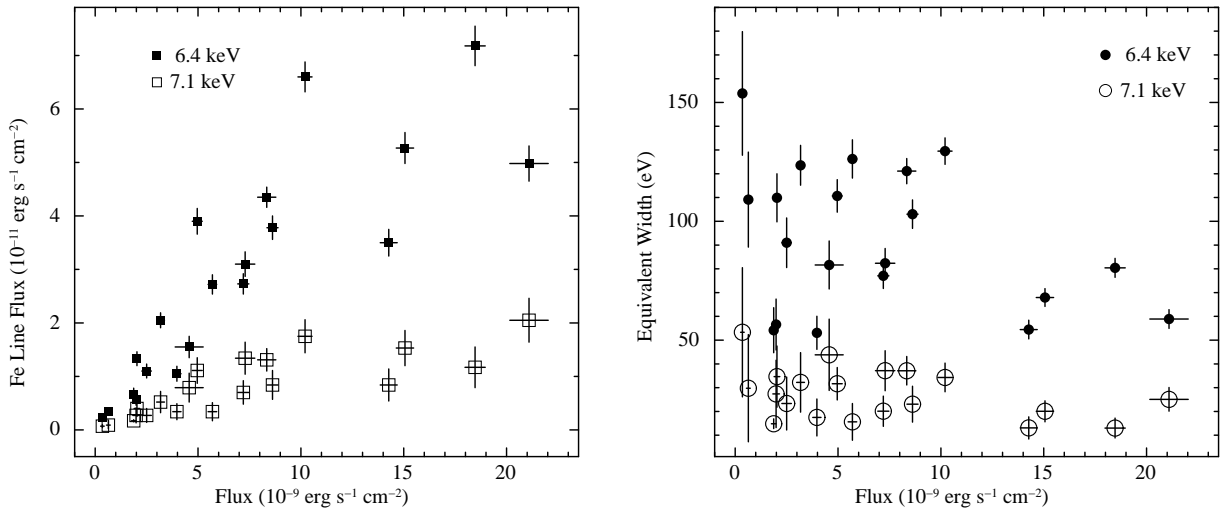


Figure 6. Change in the 6.4 keV and 7.1 keV iron emission line flux (left panel) and equivalent widths (right panel) with respect to the estimated flux in 8-70 keV energy range.

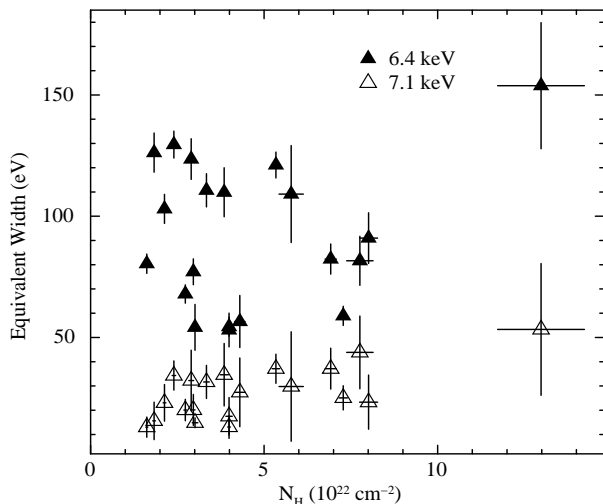


Figure 7. Change in the 6.4 keV and 7.1 keV iron line equivalent widths with respect to the column density during the *Suzaku* observation.

as Vela X-1 (Kreykenbohm et al. 2008), Cen X-3 (Naik et al. 2011), 4U 1907+09 (River et al. 2010) etc. The source luminosity in these wind-fed systems depends on the density and velocity of stellar wind as $L_x \propto \rho v^{-3}$ (Bondi & Hoyle 1944). Any fluctuations either in density or velocity can produce the variation in luminosity. Flux variability in time scales of kilo-seconds as seen in 4U 1700-37, were seen in Vela X-1 and was explained on the basis of clumpy wind with the fluctuating density causing variation in the accretion rate (Kreykenbohm et al. 2008; Odaka et al. 2013). Presence of low and high flux levels were also seen in the pulsar 4U 1907+09 during *Suzaku* observations in 2006 and 2007 (Rivers et al. 2010). Though the low flux levels were present in the light curves of both the observations, the one present in 2006 observation was consistent with earlier observations of 4U 1907+09 and interpreted as due to change in whole continuum rather than obscuration/absorption of X-rays due to the presence of additional matter as in later case (Rivers et al. 2010). The argument of presence of clump of matter causing low flux levels in the light curves during 2007 observation was supported by the enhancement in the value of absorption column density along the line of sight. However, in the present study, the variation of N_H was marginal during flare and non-flare durations. Significantly high value of N_H after orbital phase ~ 0.6 compared to rest of the segments of the *Suzaku* observation confirmed the finding from *EXOSAT* observation of the source. This high N_H value segment (beyond orbital phase of ~ 0.6) was interpreted as due to the passage of the accretion wake between the neutron star and the observer. As the neutron star moves away, the accretion wake which trails behind the neutron star during the whole orbit, crosses the line of sight of the observer at ~ 0.6 orbital phase yielding significantly high value of absorption column density.

Taam & Fryxell (1989) performed the simulation to understand the interaction between asymmetric accretion flow from OB stars onto the neutron stars. The results showed that a temporary disk can be formed during the interaction of accretion flow with the shock in accretion wake region. The destruction of temporary accretion disk is associated

with the reversal of storage accretion flow that increases the mass accretion rate. The flow reversal occurs in the range of few hours that generates the flares of 15 m to 1 hr time scales as seen in several segments (such as 3, 4, 7, 10 etc.) of present *Suzaku* observation. The “flip-flop instability” in the accretion disk can possibly also explain short time flaring activities as observed in 4U 1700-37 (Matsuda et al. 1991). However, in an alternate scenario, the hydrodynamics simulation results for wind-fed sources showed the formation of non-steady accretion wake consisting the dense filaments of compressed gas where the density reaches ~ 100 times more compared to undisturbed stellar wind (Blondin et al. 1990). Accretion of these filaments with fluctuating density may generate the abrupt variation in the X-ray luminosity as observed in the present case.

Suzaku observation of 4U 1700-37 was taken during out of eclipse of binary. However, an eclipse-like low flux segment was observed towards the end of the observation in 0.63-0.73 orbital phase range. During this segment, an increase in column density was found. The source flux and line flux of both the iron emission lines were decreased to minimum values compared to the rest of the observation. The presence of dense matter in this orbital phase range can be the possible reason for the eclipse like segments. Such type of eclipse-like segments (quiescence period) was also observed during *Chandra* observation of 4U 1700-37 around ~ 0.68 orbital phase (Boroson et al. 2003). A significant increase in the column density after phase 0.5 was also reported earlier during the *Copernicus* observation of 4U 1700-37 (Mason et al. 1976). During *EXOSAT* observation, an increasing column density was also noticed after 0.6 orbital phase of the binary (Haberl et al. 1989). The sharp increase in the column density at above orbital phase range can be interpreted as the formation of accretion wake as observed in Vela X-1 (Blondin et al. 1990). Haberl et al. (1994) also reported the presence of accretion wake based on the temperature difference observed in the soft excess component. However, the spectroscopic evidences confirmed the formation of accretion wake at late orbital phases of binary that blocks the continuum and produces the eclipse like segments (Kaper et al. 1994) which is seen in the present case of 4U 1700-37.

In summary, the observed flux variability at ks time scale during *Suzaku* observation of 4U 1700-37 can be explained on clumpiness in the stellar wind which may cause fluctuation in mass accretion rate. However, the instability in temporary disk or flip flop instability in accretion disk can also produce the flares on short time intervals as seen in light curves between 0.29-0.63 orbital phase. The extended low flux eclipse-like segment observed towards the end of the observation is interpreted as due to the presence of accretion wake.

ACKNOWLEDGMENTS

The authors would like to thank the referee for his/her constructive comments and suggestions that improved the contents of the paper. The research work at Physical Research Laboratory is funded by the Department of Space, Government of India. The authors would like to thank all the members of the *Suzaku* for their contributions in the instrument preparation, spacecraft operation, software devel-

opment, and in-orbit instrumental calibration. This research has made use of data obtained through HEASARC Online Service, provided by the NASA/GSFC, in support of NASA High Energy Astrophysics Programs.

Titarchuk L., 1994, *ApJ*, 434, 313
 van der Meer A., Kaper L., di Salvo T., Mèndez M., van der Klis M., et al. 2005, *A&A*, 432, 999
 White N. E., Swank J. H. & Holt S. S., 1983, *ApJ*, 270, 711

REFERENCES

- Ankay A., Kaper L., de Bruijne J. H. J., et al. 2001, *A&A*, 370, 170
 Becker P. A. & Wolff M. T., 2007, *ApJ*, 654, 435
 Blondin J. M., Kallman T. R., Fryxell B. A. & Taam R. E. 1990, *ApJ*, 356, 591
 Bondi H. & Hoyle F., 1944, *MNRAS*, 104, 273
 Boroson B., Vrtillek S. D., Kallman T. & Corcoran M. 2003, *ApJ*, 592, 516
 Brown G. E., Weingartner J. C. & Wijers R. A. M. J., 1996, *ApJ*, 463, 297
 Burderi L., Di Salvo T., Robba N. R., La Barbera A., Guainazzi M., 2000, *ApJ*, 530, 429
 Clark J. S., Goodwin S. P., Crowther P. A., et al. 2002, *A&A*, 392, 909
 Haberl F., White N. E. & Kallman T. R., 1989, *ApJ*, 343, 409
 Haberl F. & Day C. S. R., 1992, *A&A*, 263, 241
 Haberl F., Aoki T. & Mavromatakis F., 1994, *A&A*, 288, 796
 Hutchings J. B., Thackeray A. D., Webster B. L. & Andrews P. J. 1973, *MNRAS*, 163, 13P
 Jaisawal G. K., Naik S., Paul B. 2013, *ApJ*, 779, 54
 Jones C., Forman W., Tananbaum H., et al. 1973, *ApJ*, 181, L43
 Kaper L., Hammerschlag-Hensberge G., Zuiderwijk E. J., 1994, *A&A*, 289, 846
 Koyama K. et al., 2007, *PASJ*, 59, 23
 Kreykenbohm I., Wilms J., Kretschmar P., Torrejón J. M., Pottschmidt K., et al. 2008, *A&A*, 492, 511
 Makishima K. 1986, *The Physics of Accretion onto Compact Objects*, ed. K. P. Mason, M. G. Watson & N. E. White (Berlin: Springer), 266, 249
 Makishima K., Mihara T., Nagase F., Tanaka Y., 1999, *ApJ*, 525, 978
 Maitra C., Paul B., Naik S., 2012, *MNRAS*, 420, 2307
 Mason K. O., Branduardi G., Sanford P., 1976, *ApJ*, 203, 29
 Matsuda T., Sekino N., Sawada K., et al. 1991, *A&A*, 248, 301
 Mitsuda K. et al., 2007, *PASJ*, 59, 1
 Murakami T., Kawai N., Makishima K., Mitani K., Hayakawa S., et al. 1984, *PASJ*, 36, 691
 Naik S., Paul B., 2003, *A&A*, 401, 265
 Naik S., Paul B., Ali Z. 2011, *ApJ*, 737, 79
 Naik S., Maitra C., Jaisawal G. K., Paul B., 2013, *ApJ*, 764, 158
 Odaka H., Khangulyan D., Tanaka Y. T., Watanabe S., Takahashi T., Makishima K., 2013, *ApJ*, 767, 70
 Paul B., Naik S., 2011, *BASI*, 39, 429
 Pradhan P., Maitra C., Paul B., Islam N., Paul B. C., 2014, *MNRAS*, 442, 2691
 Press W. H., Teukolsky S. A., Vetterling W. T., & Flannery B. P., 2007, *Numerical Recipes: The Art of Scientific Computing* (Cambridge: Cambridge Univ. Press), 730
 Reynolds A. P., Owens A., Kaper L., Parmar A. N. & Segreto A., 1999, *A&A*, 349, 873
 Rivers, E., Markowitz, A., Pottschmidt, K., et al. 2010, *ApJ*, 709, 179
 Rubin B. C., Finger M. H., Harmon B. A., et al. 1996, *ApJ*, 459, 259
 Takahashi T. et al., 2007, *PASJ*, 59, 35
 Taam R. E. & Fryxell B. A., 1989, *ApJ*, 339, 297
 Tanaka Y. 1986, in *Proc. IAU Colloq. 89, Vol. 255, Radiation Hydrodynamics in Stars and Compact Objects*, ed. D. Mihalas & K.-H. A. Winkler